J. Fluid Mech. (1994), *vol.* 263, *pp.* 207–226

Stokes flow through periodic orifices in a channel

By Y. ZENG AND S. WEINBAUM†

Department of Mechanical Engineering, The City College of the City University of New York, New York, NY 10031, USA

(Received 25 March 1993 and in revised form 13 September 1993)

This paper develops a three-dimensional infinite series solution for the Stokes flow through a parallel walled channel which is obstructed by a thin planar barrier with periodically spaced rectangular orifices of arbitrary aspect ratio B'/d' and spacing D'. Here B' is the half-height of the channel and d' is the half-width of the orifice. The problem is motivated by recent electron microscopic studies of the intercellular channel between vascular endothelial cells which show a thin junction strand barrier with discontinuities or breaks whose spacing and width vary with the tissue. The solution for this flow is constructed as a superposition of Hasimoto's (1958) general solution for the two-dimensional flow through a periodic slit array in an infinite plane wall and a new three-dimensional solution which corrects for the top and bottom boundaries. In contrast to the well-known solutions of Sampson (1891) and Hasimoto (1958) for the flow through zero-thickness orifices of circular or elliptic cross-section or periodic slits in an infinite plane wall, which exhibit characteristic viscous velocity profiles, the present bounded solutions undergo a fascinating change in behaviour as the aspect ratio B'/d' of the orifice opening is increased. For $B'/d' \ll 1$ and $(D'-d')/B'$ of $O(1)$ or greater, which represents a narrow channel, the velocity has a minimum at the orifice centreline, rises sharply near the orifice edges and then experiences a boundary-layer-like correction over a thickness of $O(B')$ to satisfy no-slip conditions. For B'/d' of $O(1)$ the profiles are similar to those in a rectangular duct with a maximum on the centreline, whereas for $B'/d' \gg 1$, which describes widely separated channel walls, the solution approaches Hasimoto's solution for the periodic infinite-slit array. In the limit $(D'-d')/B' \ll 1$, where the width of the intervening barriers is small compared with the channel height, the solutions exhibit the same behaviour as Lee & Fung's (1969) solution for the flow past a single cylinder. The drag on the zero-thickness barriers in this case is nearly the same as for the cylinder for all aspect ratios.

1. Introduction

The problem of viscous flow past a single obstacle in a closely spaced parallel-walled channel first attracted widespread attention nearly 100 years ago. In 1898, Hele-Shaw discovered that the streamlines for flow past a circular cylindrical post confined between two closely spaced parallel flat plates accurately reproduced the lines of force around a metal cylinder in a magnetic field. This phenomenon was then explained by Stokes, who mathematically proved that if the spacing between the walls $2B'$ was sufficiently small compared to the diameter $2a$ of the cylinder, the vertical component of the velocity could be neglected and the governing equation for the viscous flow in planes parallel to the boundaries became a potential flow equation. However, as a potential flow cannot satisfy the no-slip condition on the surface of the cylinder, the analysis is incomplete and becomes invalid in the region near the boundary of the

† Author to whom correspondence should be addressed.

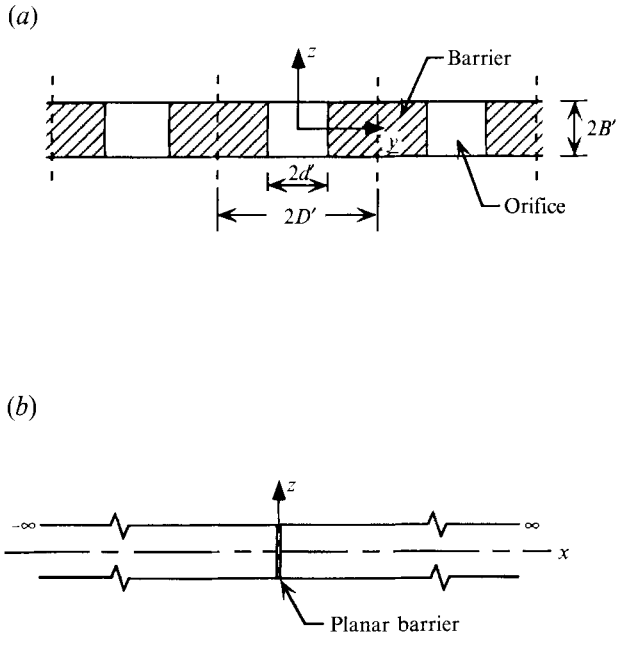

FIGURE 1. Flow geometry showing (*a*) frontal view of a barrier in the plane $x = 0$ and (*b*) side view of a barrier in an infinite channel in the plane $y = 0$.

cylinder. Using singular perturbation theory, Thompson (1968) showed that for $B'/a \ll 1$ and a of $O(1)$ there was a thin layer near the cylinder of thickness $O(B')$ where the vertical velocity did not vanish and the viscous terms could not be neglected owing to the requirement of the no-slip boundary conditions. Important advances in the analysis of this problem were then made by Lee & Fung (1969) who obtained the Stokes solution for three-dimensional flow past a single circular cylinder in studying the flow of blood around a septal post in pulmonary alveoli where the aspect ratio of the post B'/a was typically $O(1)$. This solution was then extended by Lee (1969) to a doubly periodic array of cylinders using a two-term approximation that provided reasonable numerical results provided $B'/a \leqslant O(1)$ and the cylinder spacing $D'/a \gg 1$. This same problem has recently been re-examined by Tsay & Weinbaum (1991) who were interested in the flow through perpendicular fibre arrays in a channel as a model for filtration flow in capillary interendothelial clefts (Tsay, Weinbaum & Pfeffer 1989). To achieve this objective these investigators developed a truncated infinite series solution that extended Lee & Fung's analysis to periodic cylinders of arbitrary aspect ratio and spacing. This new class of solutions successfully described the transition in behaviour from the Hele-Shaw potential flow limit (aspect ratio $B'/a \ll 1$) to the viscous two-dimensional limit, $B'/a \gg 1$ (Sangani & Acrivos 1982) for the hydrodynamic interaction between the fibres. These previous solutions for the flow past a single circular cylinder of Lee & Fung (1969), or a doubly periodic array of cylinders (Tsay & Weinbaum 1991), have been derived by truncating a general series solution which satisfies the governing equations and no-slip boundary conditions on the walls associated with both the channel boundaries and the cylinders.

In the present study, we shall investigate the orifice flow through a planar periodic array of barriers of width $2(D'-d')$ and height $2B'$ between two parallel walls, as shown in figure 1. We develop a new general solution which is a superposition of Hasimoto's (1958) classical solution for Stokes flow through a periodic infinite-slit

array in an unbounded plane wall and a new three-dimensional infinite series solution which corrects for the top and bottom boundaries. In particular, the new general solution satisfies the governing equations and all boundary conditions except the zero normal velocity component on the barriers and a zero pressure symmetry condition at orifice openings. The latter condition is then satisfied by truncating a single infinite series of remaining unknown coefficients. This new solution converges rapidly for orifices of all aspect ratios, from $B = B'/d' \ll 1$ to $B \gg 1$, provided $D = D'/d'$ is less than approximately 5. In the limit $B \ll 1$ and $(D-1) \sim O(1)$, the flow can be simply approximated by a Hele-Shaw potential flow equation, and solved exactly by conformal mapping methods. This solution is singular near the edges of the orifice, and in contrast to the classical solution of Sampson (1891) for viscous flow through a circular orifice in a plane wall has a minimum velocity at the centreline. Three-dimensional corrections are required in a region of $O(B')$ near the edges to satisfy viscous flow boundary conditions. When $B \sim O(1)$ the solution of the full Stokes equations exhibits three-dimensional behaviour throughout the region of the orifice. The limiting case $B \gg 1$ corresponds to the exact two-dimensional solution given by Hasimoto (1958) for the flow through an infinite plate with periodic slits. We believe that the new solutions given herein are of fundamental interest to fluid mechanicians because they described the transition in behaviour from the irrotational Hele-Shaw potential flow limit to Hasimoto's two-dimensional limiting behaviour as B increases from $B \ll 1$ to $B \gg 1$. In addition, when $(D-1) \ll 1$, one approaches the limiting behaviour examined by Lee & Fung (1969) for the flow past an isolated cylinder of arbitrary aspect ratio.

The motivation for the present study derives from a recent paper by Weinbaum, Tsay & Curry (1992) in which a three-dimensional theoretical model is proposed for the ultrastructure of the clefts (channel) between adjacent endothelial cells. This model is based on the electron microscopic studies of Bundgaard (1984) and Adamson & Michel (1993) for the three-dimensional organization of the junction strand barrier which modulates the flow of water and solutes across the cleft. In contrast to an earlier model proposed in Tsay *et al.* (1989), where the pores in the junction strand were viewed as circular holes of $5 \sim 6$ nm radius, the new model in Weinbaum *et al.* (1992) predicts that the most likely pore is a $40 \sim 200$ nm wide break in the junction strand whose height, $2B' \sim 20$ nm, is the spacing between the plasmalemma boundaries of the cleft. This prediction has just been confirmed by the three-dimensional serial section electron microscopic reconstructions of frog mesentery capillaries reported in Adamson & Michel (1993). For these dimensions $0.1 < B < 0.5$, and it is necessary to develop a model that considers an orifice that spans the behaviour from the Hele-Shaw limit $B \ll 1$ to $B \sim O(1)$.

This paper is presented in six sections. Section 2 describes the new three-dimensional solutions of the Stokes creeping flow equations for the flow geometry shown in figure 1. The conforming mapping solution for the Hele-Shaw limit is presented in §3. In §4 the principal results are shown and the Stokes solutions are compared with the various asymptotic solutions described in this introduction. Finally, a brief discussion of biological application and the conclusions are given in §§5 and 6.

2. Three-dimensional Stokes solution for flow through a periodic orifice in a channel

2.1. *Governing equations and boundary conditions*

The dimensionless governing equations and boundary conditions for the incompressible Stokes flow shown in figure 1 can be written as follows:

$$\nabla \cdot \boldsymbol{v} = 0, \tag{1}$$

$$\nabla^2 \boldsymbol{v} = \nabla p, \tag{2}$$

and

$$\boldsymbol{v} \sim \boldsymbol{i}(1 - z^2/B^2) \quad \text{as} \quad x \to \infty, \tag{3a}$$

$$\boldsymbol{v} = 0 \quad \text{at} \quad z = \pm B, \tag{3b}$$

$$v_y = 0 \quad \text{at} \quad y = \pm D, \tag{3c}$$

$$v_y = v_z = 0 \quad \text{at} \quad x = 0, \tag{3d}$$

$$v_x = 0 \quad \text{at} \quad x = 0, \quad 1 \leqslant |y| \leqslant D, \tag{3e}$$

$$p = 0 \quad \text{at} \quad x = 0, \quad 0 \leqslant |y| \leqslant 1. \tag{3f}$$

The dimensionless quantities are defined as

$$\boldsymbol{x} = \boldsymbol{x}'/d', \quad D = D'/d', \quad B = B'/d', \quad \boldsymbol{v} = \boldsymbol{v}'/(Q/D'B'), \quad p = p'/(\mu Q/d'D'B'),$$

where Q is the flow in the periodic unit, $-D \leqslant y \leqslant D$, and μ is the viscosity of the fluid.

To solve the flow problem defined by (1)–(3), we shall first find a general solution which satisfies all the boundary conditions except (3*e*) and (3*f*) and then apply these two remaining boundary conditions to determine the unknown constants in a truncated infinite series that accurately approximates the exact solution for most cases of interest.

2.2. *General solution*

Hasimoto (1958) proposed a set of general solutions for the Stokes equations, which is the most appropriate form to describe flow past an infinite plane with an arbitrary arrangement of holes or slits. However, this general solution $\boldsymbol{v}_h$ does not satisfy the boundary condition on the walls at $z = \pm B$. Therefore, a new three-dimensional solution must be constructed which has the flexibility to cause all three velocity components to vanish and also satisfy conditions (3*a*, *c*, *d*). This superposition is given by

$$\boldsymbol{v} = \boldsymbol{v}_\infty + \boldsymbol{v}_h + \boldsymbol{v}_c$$

where $\boldsymbol{v}_\infty$ is the Poiseuille flow at infinity.

The general solution of Stokes equation that satisfies $v_y = v_z = 0$ at $x = 0$ is given in Hasimoto (1958) as

$$\boldsymbol{v}_h = \boldsymbol{i}\phi - x\nabla\phi, \quad p_h = -2\,\partial\phi/\partial x, \tag{4a, b}$$

where ϕ satisfies

$$\Delta\phi = 0. \tag{5}$$

A separable solution for ϕ that satisfies $v_x = v_y = 0$ at $z = \pm B$ and $v_y = 0$ at $y = \pm D$ is

$$\phi = \sum_{n=0}^{\infty} \sum_{m=0}^{\infty} A_{nm}\, \mathrm{e}^{-\gamma_{nm} x} \cos\frac{m\pi y}{D} \cos k_n z,$$

where $k_n = (2n+1)\,\pi/(2B)$ and $\gamma_{nm}^2 = k_n^2 + (m\pi/D)^2$. The general solution for $\boldsymbol{v}_h$ and p_h can be expressed in the following form:

$$v_{hx} = \sum_{n=0}^{\infty} \sum_{m=0}^{\infty} A_{nm}(1 + \gamma_{nm}|x|)\, \mathrm{e}^{-\gamma_{nm}|x|} \cos\frac{m\pi y}{D} \cos k_n z, \tag{6a}$$

$$v_{hy} = \sum_{n=0}^{\infty} \sum_{m=0}^{\infty} A_{nm} \frac{m\pi}{D} x \, e^{-\gamma_{nm}|x|} \sin \frac{m\pi y}{D} \cos k_n z, \tag{6b}$$

$$v_{hz} = \sum_{n=0}^{\infty} \sum_{m=0}^{\infty} A_{nm} k_n x \, e^{-\gamma_{nm}|x|} \cos \frac{m\pi y}{D} \sin k_n z, \tag{6c}$$

$$p_h = \sum_{n=0}^{\infty} \sum_{m=0}^{\infty} 2A_{nm} \gamma_{nm} e^{-\gamma_{nm}|x|} \cos \frac{m\pi y}{D} \cos k_n z \frac{|x|}{x}. \tag{6d}$$

This general solution with correct symmetries of geometry about $x = 0$ still needs to satisfy no-slip boundary conditions for v_z on the walls, the zero normal velocity at the barriers, $x = 0$, as well as the zero pressure condition (3*f*).

We next consider a second solution to Stokes equation that satisfies $v_x = v_y = 0$ at $z = \pm B$. Following the general approach in Lee & Fung (1969), we assume a solution in the form

$$v_{cx} = \frac{1}{\alpha^2} \frac{\partial \psi}{\partial x} \frac{dq}{dz}, \quad v_{cy} = \frac{1}{\alpha^2} \frac{\partial \psi}{\partial y} \frac{dq}{dz}, \quad v_{cz} = \psi(x, y) q(z). \tag{7a–c}$$

When (7*a–c*) are substituted into the continuity equation, one obtains the following kinematic constraint:

$$\frac{\partial^2 \psi}{\partial x^2} + \frac{\partial^2 \psi}{\partial y^2} + \alpha^2 \psi = 0. \tag{8}$$

If one now also substitutes (7*a–c*) into the Stokes equation and employs (8), one finds that for the pressure to be compatible in all directions

$$\frac{d^4 q}{dz^4} - 2\alpha^2 \frac{d^2 q}{dz^2} + \alpha^4 q(z) = 0. \tag{9}$$

The solution of (8) that satisfies the boundary condition $v_y = 0$ at $y = \pm D$ as well as $v_y = v_z = 0$ at $x = 0$ is

$$\psi = \sum_{m=0}^{\infty} B_m \sin \omega x \cos \frac{m\pi y}{D}, \tag{10}$$

where $$\omega^2 = \alpha^2 - (m\pi/D)^2.$$

The solution of (9) that satisfies the boundary conditions $v_x = v_y = 0$ at $z = \pm B$ is

$$q(z) = \frac{\sinh \alpha z}{\alpha \cosh \alpha B} + \frac{\sinh \alpha z}{\alpha^2 B \sinh \alpha B} - \frac{z \cosh \alpha z}{\alpha B \sinh \alpha B}. \tag{11}$$

Finally, combining (7), (10) and (11) we obain another general solution of the Stokes equations:

$$v_{cx} = \sum_{m=0}^{\infty} \cos \frac{m\pi y}{D} \int_0^{\infty} \frac{1}{\alpha^2} \omega B_m(\omega) \cos \omega x \frac{dq}{dz} d\omega, \tag{12a}$$

$$v_{cy} = -\sum_{m=0}^{\infty} \frac{m\pi}{D} \sin \frac{m\pi y}{D} \int_0^{\infty} \frac{1}{\alpha^2} B_m(\omega) \sin \omega x \frac{dq}{dz} d\omega, \tag{12b}$$

$$v_{cz} = \sum_{m=0}^{\infty} \cos \frac{m\pi y}{D} \int_0^{\infty} B_m(\omega) (q(z) \sin \omega x) \, d\omega, \tag{12c}$$

$$p_c = -\sum_{m=0}^{\infty} \cos \frac{m\pi y}{D} \int_0^{\infty} B_m(\omega) \sin \omega x \frac{2 \cosh \alpha z}{\alpha B \sinh \alpha B} d\omega. \tag{12d}$$

It is important to observe that solution v_c possesses appropriate symmetry properties at $x = 0$. We should mention that if the negative sign is chosen instead of the positive one on the right-hand sides of (7*a*) and (7*b*), a similar analysis to that shown above would have led to Lee & Fung's solution, equations (8) and (10) in their paper, which does not have the desired symmetry properties at $x = 0$.

The no-slip boundary conditions on the walls have been satisfied by the general solutions (6) and (12) except for $v_z = 0$. The later condition provides an analytical relationship between A_{nm} and $B_m(\omega)$,

$$\sum_{n=0}^{\infty} A_{nm} k_n x \,\mathrm{e}^{-\gamma_{nm}|x|} \sin k_n + \int_0^{\infty} B_m(\omega)\,(q(B) \sin \omega x)\,\mathrm{d}\omega = 0. \tag{13}$$

Taking the inverse Fourier transform of (13), we obtain

$$B_m(\omega) = -\frac{2}{\pi} \sum_{n=0}^{\infty} A_{nm}(-1)^n k_n I_{nm}(\omega), \tag{14}$$

where $$I_{nm} = \frac{1}{q(B)} \int_0^{\infty} x \,\mathrm{e}^{-\gamma_{nm} x} \sin \omega x \,\mathrm{d}x = \frac{2\gamma_{nm}\,\omega\alpha^2 B/(\gamma_{nm}^2 + \omega^2)^2}{(1 + \alpha B(\tanh \alpha B - \coth \alpha B))}.$$

Combining (6), (12) and (14), the general solution can be written as

$$v_x = 1 - \frac{z^2}{B^2} + \sum_{n=0}^{\infty} \sum_{m=0}^{\infty} A_{nm} \cos \frac{\mathrm{m}\pi y}{D} \left[(1 + \gamma_{nm}|x|)\,\mathrm{e}^{-\gamma_{nm}|x|} \cos k_n z - (-1)^n \frac{2}{\pi} k_n I_{nm}^{(1)}(x, z) \right], \tag{15a}$$

$$v_y = \sum_{n=0}^{\infty} \sum_{m=0}^{\infty} A_{nm} \frac{m\pi}{D} \sin \frac{m\pi y}{D} \left[x \,\mathrm{e}^{-\gamma_{nm}|x|} \cos k_n z + (-1)^n \frac{2}{\pi} k_n I_{nm}^{(2)}(x, z) \right], \tag{15b}$$

$$v_z = \sum_{n=0}^{\infty} \sum_{m=0}^{\infty} A_{nm} k_n \cos \frac{m\pi y}{D} \left[x \,\mathrm{e}^{-\gamma_{nm}|x|} \sin k_n z - (-1)^n \frac{2}{\pi} I_{nm}^{(3)}(x, z) \right], \tag{15c}$$

$$p = \sum_{n=0}^{\infty} \sum_{m=0}^{\infty} 2A_{nm} \cos \frac{m\pi y}{D} \left[\gamma_{nm} \,\mathrm{e}^{-\gamma_{nm}|x|} \cos k_n z \frac{|x|}{x} + (-1)^n \frac{2}{\pi} k_n I_{nm}^{(4)}(x, z) \right] - \frac{2x}{B^2}, \tag{15d}$$

where

$$I_{nm}^{(1)}(x, z) = \int_0^{\infty} \frac{1}{\alpha^2} \omega I_{nm}(\omega) \cos \omega x \frac{\mathrm{d}q(z)}{\mathrm{d}z} \mathrm{d}\omega,$$

$$I_{nm}^{(2)}(x, z) = \int_0^{\infty} \frac{1}{\alpha^2} I_{nm}(\omega) \sin \omega x \frac{\mathrm{d}q(z)}{\mathrm{d}z} \mathrm{d}\omega,$$

$$I_{nm}^{(3)}(x, z) = \int_0^{\infty} I_{nm}(\omega)\,(q(z) \sin \omega x)\,\mathrm{d}\omega,$$

$$I_{nm}^{(4)}(x, z) = \int_0^{\infty} I_{nm}(\omega) \sin \omega x \frac{2 \cosh \alpha z}{\alpha B \sinh \alpha B} \mathrm{d}\omega.$$

The newly derived general solution (15*a–d*) satisfies the governing equations and all boundary conditions except the mixed boundary condition $v_x = 0$ at $x = 0, 1 \leqslant |y| \leqslant D$ and $p = 0$ at $x = 0$, $|y| \leqslant 1$.

Note that the velocity expression at $x = 0$ in the general solution (15*a*) has no

orthogonality about z, but the pressure expression (15d) does. We, therefore, expand the pressure on the barrier $1 \leqslant |y| \leqslant D$ as

$$p_w = \sum_{n=0}^{\infty} \sum_{m=0}^{\infty} 2C_{nm} \sin \beta_m (y-1) \cos k_n z, \tag{16}$$

where $\beta_m = (2m+1)\pi/[2(D-1)]$, so that the pressure is continuous at the edge of the barrier, since $p_w = 0$ at $y = 1$, and satisfies the periodicity in the y-direction. From (3f) and (15d), we can write

$$\sum_{n=0}^{\infty} \sum_{m=0}^{\infty} 2A_{nm} \gamma_{nm} \cos \frac{m\pi y}{D} \cos k_n z = \begin{cases} p_w, & 1 \leqslant |y| \leqslant D \\ 0, & |y| \leqslant 1. \end{cases}$$

Applying the orthogonality of Fourier's series, we obtain

$$A_{nm} = \frac{a_m}{\gamma_{nm}} \sum_{j=0}^{\infty} C_{nj} f_{jm}, \tag{17}$$

where

$$a_m = \begin{cases} 2/D & \text{if} \quad m \neq 0 \\ 1/D & \text{if} \quad m = 0, \end{cases}$$

$$f_{jm} = \int_1^D \sin \beta_j (y-1) \cos \frac{m\pi y}{D} \, \mathrm{d}y$$

$$= \begin{cases} \dfrac{\beta_j}{\beta_j^2 - (m\pi/D)^2} \cos \dfrac{m\pi}{D} & \text{if} \quad \beta_j \neq \dfrac{m\pi}{D} \\ -\dfrac{D-1}{2} \sin \dfrac{m\pi}{D} + \dfrac{D}{4m\pi} \cos \dfrac{m\pi}{D} & \text{if} \quad \beta_j = \dfrac{m\pi}{D}. \end{cases}$$

The only remaining boundary condition to be satisfied is $v_x = 0$ in $1 \leqslant |y| \leqslant D$ at $x = 0$. From (15a) and (17), this condition requires

$$\sum_{n=0}^{\infty} \sum_{m=0}^{\infty} C_{ij} \left[\sum_{k=0}^{\infty} \frac{a_k}{\gamma_{ik}} f_{jk} \cos \frac{k\pi y}{D} (\cos k_i z - \frac{2(-1)^i}{\pi} k_i I_{ik}^{(1)}(0, z)) \right] = -\left(1 - \frac{z^2}{B^2}\right). \tag{18}$$

Equation (18) is now multiplied by $\cos k_n z$ and $\sin \beta_m (y-d)$ and then integrated over the intervals $-1 \leqslant z \leqslant 1$ and $1 \leqslant y \leqslant D$. This leads to a linear matrix of equations for the only remaining set of unknown coefficients, the C_{ij}:

$$\sum_{i=0}^{\infty} \sum_{j=0}^{\infty} C_{ij} g_{ijnm} = -\frac{4(-1)^n}{k_n^3} f_{m0}, \tag{19}$$

where

$$g_{ijnm} = \delta_{in} \sum_{k=0}^{\infty} \frac{a_k f_{jk} f_{mk}}{\gamma_{ik}} - \sum_{k=0}^{\infty} \frac{2(-1)^i k k_i f_{jk} f_{mk}}{D \gamma_{ik}} e_{ink},$$

$$e_{ink} = 2 \int_0^B I_{ik}^{(1)}(0, z) \cos k_n z \, \mathrm{d}z$$

$$= 8(-1)^n k_n \gamma_{ik} \int_0^{\infty} \frac{\omega^2 \alpha_k \coth \alpha_k B}{(\omega^2 + \gamma_{ik}^2)^2 (\omega^2 + \gamma_{nk}^2)^2 [1 + \alpha_k B(\tanh \alpha_k B - \coth \alpha_k B)]} \mathrm{d}\omega,$$

$$\gamma_{ik} = [k_i^2 + (k\pi/D)^2]^{\frac{1}{2}},$$

$$\alpha_k^2 = \omega^2 + (k\pi/D)^2.$$

The double series in (19) is now truncated and solved by standard matrix reduction schemes. The convergence of this solution is examined in §4.1.

2.3. *The resistance to the flow*

The total resistance to the flow consists of two parts: the shear stress applied by the walls F_w and the force applied by the barrier F_b.

Because of the antisymmetric nature of pressure field, equation (15*d*), and its symmetry about $y = z = 0$, the drag acting on the barrier is eight times the force in the region $0 \leqslant z \leqslant B$, $1 \leqslant y \leqslant D$:

$$F_b = -\frac{8\mu Q}{d'DB}\int_0^B\int_1^D \tau_{xx}|_{x=0^+}\,\mathrm{d}z\,\mathrm{d}y$$

$$= \frac{16\mu Q}{d'DB}\sum_{n=0}^{\infty}\sum_{m=0}^{\infty}\frac{(-1)^n C_{nm}}{k_n\beta_m}, \tag{20}$$

where $\tau_{xx} = -p + 2\,\partial v_x/\partial x$. In view of the no-slip boundary condition on the barrier and the continuity equation, $\tau_{xx} = -p_w$.

The drag force acting on the barrier can be described by a dimensionless coefficient:

$$f_b = \frac{F_b}{4\mu Q/D'} = \frac{4}{B}\sum_{n=0}^{\infty}\sum_{m=0}^{\infty}\frac{(-1)^n C_{nm}}{k_n\beta_m}. \tag{21}$$

From (15*a*) and (17), the frictional resistance on the two walls, from the upstream position $x' = -L'$ to its downstream image plane $x' = L'$, within the periodic unit $-D' \leqslant y' \leqslant D'$ can be expressed as

$$F_w = \frac{8\mu Q}{d'DB}\int_0^L\int_0^D \tau_{xz}|_{z=B}\,\mathrm{d}x\,\mathrm{d}y$$

$$= -\frac{8\mu Q}{d'B}\left[\frac{2L}{B} + 2\sum_{n=0}^{\infty}\sum_{m=0}^{\infty}\frac{(-1)^n C_{nm}}{Dk_n\beta_n}\left(1 - k_n L\,\mathrm{e}^{-k_n L} - \mathrm{e}^{-k_n L}\right.\right.$$

$$\left.\left. - \frac{2k_n}{\pi}\int_0^{\infty}\frac{I_{n0}(\omega)\sin\omega L}{\omega B\sinh\omega B\cosh\omega B}\,\mathrm{d}\omega\right)\right], \tag{22}$$

where $\tau_{xz} = \partial v_x/\partial z$. Two terms lie within the square brackets on the right-hand side of (22). The first term represents the resistance due to the undisturbed Poiseuille flow. Therefore, one concludes that the friction force on the walls due to the disturbance produced by the barrier is due to the second term involving the double summation. The integral in the second term tends to zero as L tends to infinity according to the Riemann–Lebesque lemma (see Zauderer 1989). If we now let L tend to infinity in the double summation and compare the resulting force contribution for F_w, we find it is identical to the drag applied on the barrier, equation (20). The total additional frictional force on the walls at $z = \pm B$ due to the presence of the barrier is thus the same as the result given by (20).

3. An exact solution for Hele-Shaw flow

We now consider a simpler model for the limit $B \ll 1$. We assume that the flow moves as parallel sheets in the (x, y)-plane and neglect regions of $O(B')$ near the barrier. In this exterior flow region, the Hele-Shaw potential flow equation applies. The dimensionless governing equations and boundary conditions are

$$\boldsymbol{v} = -\tfrac{1}{2}B^2\,\nabla p(1 - z^2/B^2), \tag{23}$$

$$\nabla^2 p = 0, \tag{24}$$

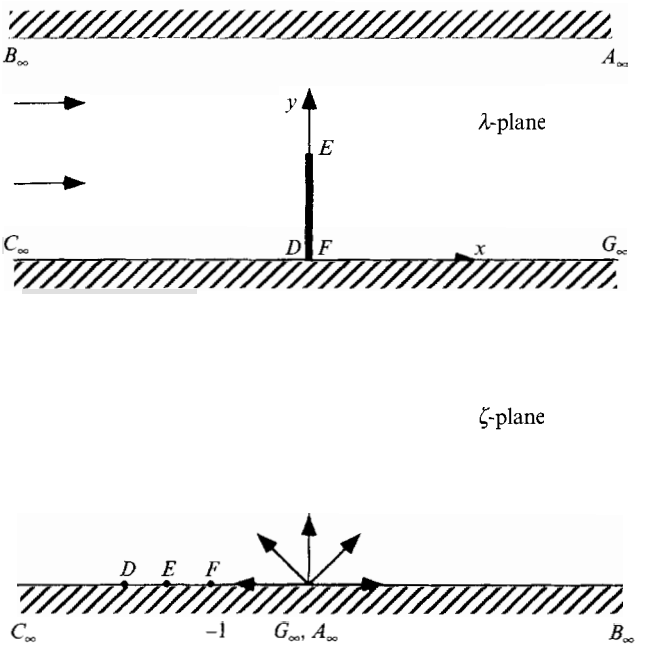

FIGURE 2. Sketch of two-dimensional Hele-Shaw potential flow showing the transformation from the λ-plane to the ζ-plane for the asymptotic case $B \ll 1$.

and
$$\frac{\partial p}{\partial x} = 0 \quad \text{at} \quad x = 0, \quad 1 \leqslant y \leqslant D, \tag{25a}$$

$$-\frac{2}{B^2}, \quad \frac{\partial p}{\partial y} = 0 \quad \text{as} \quad x \tag{25b}$$

As shown in figure 2, the physical λ-plane can be mapped into the ζ-plane using a Schwartz–Christofel conformal transformation:

$$\lambda = -\frac{D}{\pi}\ln\left(-\frac{\{\zeta+\zeta_3+[(\zeta+\zeta_3^2)(\zeta+1)]^{\frac{1}{2}}\}^2}{\zeta(\zeta_3-1)^2}\right), \quad \lambda = x+\mathrm{i}y. \tag{26}$$

Equation (26) transforms the flow in the infinite strip $0 \leqslant y \leqslant D$ in the physical plane into the upper half-plane of the ζ-plane with a line source at the origin. The corresponding inverse transformation is:

$$\zeta = \tfrac{1}{2}[-b-(b^2-4\zeta_3^2)^{\frac{1}{2}}], \tag{27}$$

where
$$b = b(\lambda) = \tfrac{1}{2}[(1-\zeta_3)^2\cosh(\pi\lambda/D)+(1+\zeta_3)^2],$$

$$\zeta_3 = -\frac{1+\sin\pi/2D}{(1-\sin\pi/2D)}.$$

The complex potential in the ζ-plane is

$$W = \frac{2D}{\pi B^2}\ln\zeta + C.$$

Therefore the stream function is

$$\Psi = \frac{2D}{\pi B^2}[\mathrm{Im}\,(\ln \zeta) - \pi] \tag{28}$$

and the pressure is

$$p = \frac{2D}{\pi B^2}[\mathrm{Re}\,(\ln \zeta) - \ln(-\zeta_3)]. \tag{29}$$

The complex velocity is given by

$$\frac{\mathrm{d}W}{\mathrm{d}\lambda} = -\frac{2}{B^2}\frac{[(\zeta+\zeta_3^2)(\zeta+1)]^{\frac{1}{2}}}{\zeta-\zeta_3}. \tag{30}$$

From (23) and (30) the x and y velocity components are

$$v_x = -\frac{B^2}{2}\left(1-\frac{z^2}{B^2}\right)\mathrm{Re}\left(\frac{\mathrm{d}W}{\mathrm{d}\lambda}\right), \quad v_y = \frac{B^2}{2}\left(1-\frac{z^2}{B^2}\right)\mathrm{Im}\left(\frac{\mathrm{d}W}{\mathrm{d}\lambda}\right). \tag{31a, b}$$

The drag force acting on the barrier for the Hele-Shaw potential flow is obtained by integrating (29) over the surface:

$$F_b = \frac{8\mu Q}{dDB}\int_0^B\int_1^D p|_{x=0^+}\,\mathrm{d}z\,\mathrm{d}y = \frac{16\mu Q}{\pi d B^2}\int_1^D [\mathrm{Re}\,(\ln\zeta) - \ln(-\zeta_3)]\,\mathrm{d}y.$$

The corresponding dimensionless friction coefficient is

$$f_b = \frac{F_b}{4\mu Q/D'} = \frac{4D}{\pi B^2}\int_1^D [\mathrm{Re}\,(\ln(\zeta) - \ln(-\zeta_3)]\,\mathrm{d}y. \tag{32}$$

We should mention that the term $\partial v_x/\partial x$ in the normal stress, $\tau_{xx} = -p + 2\,\partial v_x/\partial x$, acting on the barrier at $x = 0$ has been neglected because the Hele-Shaw approximation violates the no-slip boundary condition on the v_y component of the velocity at the barrier. The normal force is approximated by the pressure field outside the viscous correction layer as in boundary-layer theory.

4. Results

In this section, we will discuss the convergence of the solutions, present representative solutions for the velocity profiles, compare these results with asymptotic solutions and plot the numerical results for the drag coefficient f_b.

4.1. *Convergence of the solutions*

The only boundary condition that needs to be satisfied numerically is condition (3*e*) for the normal velocity component at the barrier. Our criterion for convergence is that $|v_x|$ does not exceed a prescribed error tolerance at selected points on the barrier. The unknown coefficients C_{nm} in (19) are functions of B and D.

The convergence of the truncated matrix solution as M and N are increased for $B = 0.1$, 1 and 10 and $D = 2$ are shown in table 1. Values of v_x at two points on the barrier, p_1 and p_2, with the coordinates $(0, \frac{1}{2}(D+1), \frac{1}{2}B)$ and $(0, \frac{1}{2}(D+1), 0)$ are listed in this table. For $B = 1$ there is faster convergence along the diagonal than for $B = 0.1$

M	Point	$N=4$	$N=6$	$N=10$	$N=12$	$N=14$	$N=16$
				(*a*) $B=0.1$			
20	p_1	0.0591	0.0443	0.0476	0.0497	0.0482	0.0493
	p_2	0.0167	0.0369	0.0494	0.0524	0.0537	0.0553
50	p_1	−0.0477	−0.0162	−0.0129	−0.0112	—	—
	p_2	−0.0559	−0.0358	−0.0230	−0.0204	—	—
100	p_1	0.0158	0.0003	—	—	—	—
	p_2	−0.0369	−0.0165	—	—	—	—
				(*b*) $B=1$			
20	p_1	0.0152	0.0098	0.0107	0.0116	0.0110	0.0113
	p_2	−0.0015	0.0057	0.0100	0.0113	0.0114	0.0120
50	p_1	0.0013	−0.0042	−0.0032	−0.0023	—	—
	p_2	−0.0185	−0.0110	−0.0066	−0.0054	—	—
100	p_1	0.0051	−0.0004	—	—	—	—
	p_2	−0.0139	−0.0066	—	—	—	—
				(*c*) $B=10$			
20	p_1	0.0228	0.0033	0.0077	0.0098	0.0080	0.0091
	p_2	−0.0436	−0.0186	−0.0032	0.0006	0.0031	0.0044
50	p_1	0.1190	−0.0074	−0.0032	−0.0008	—	—
	p_2	−0.0560	−0.0318	−0.0148	−0.0110	—	—
100	p_1	0.0148	−0.0050	—	—	—	—
	p_2	−0.0532	−0.0274	—	—	—	—

TABLE 1. Convergence tests for $v_x = 0$ at points p_1 and p_2 on the barrier for $D = 2$

M	$N=4$	$N=6$	$N=8$	$N=10$	$N=12$	$N=14$	$N=16$
				(*a*) $B=0.1$			
20	428.8	438.0	442.8	445.6	447.6	448.8	450.0
30	433.6	442.8	447.6	450.4	452.0	453.6	454.4
40	436.0	445.2	450.0	452.8	454.8	456.0	—
50	437.2	446.8	451.6	454.4	456.4	—	—
100	440.4	449.6	—	—	—	—	—
				(*b*) $B=1$			
20	19.45	19.70	19.84	19.93	19.99	20.03	20.06
30	19.68	19.94	20.08	20.17	20.22	20.27	20.30
40	19.80	20.06	20.20	20.29	20.35	20.39	—
50	19.87	20.13	20.35	20.36	20.42	—	—
100	20.02	20.28	—	—	—	—	—
				(*c*) $B=10$			
20	11.55	11.71	11.78	11.83	11.86	11.88	11.90
30	11.67	11.86	11.94	11.98	12.02	12.04	12.05
40	11.76	11.93	12.02	12.06	12.09	12.11	—
50	11.80	11.98	12.06	12.11	12.14	—	—
100	11.90	12.07	—	—	—	—	—

TABLE 2. Convergence tests for friction factor f_b for $D = 2$

or 10. Thus, for $B = O(1)$ the truncation order is important in both N and M. However, table 1 (*a*) and table 1 (*c*) illustrate that more efficient convergence is achieved by letting M increase for $B \ll 1$ and letting N increase for $B \gg 1$. Typically, the errors for the three cases do not exceed 1 % when $N \geqslant 12$ and $M \geqslant 50$. When $D \gg 1$, the convergence is rather slow. For instance, when $D = 10$ (results not shown to save space) the error

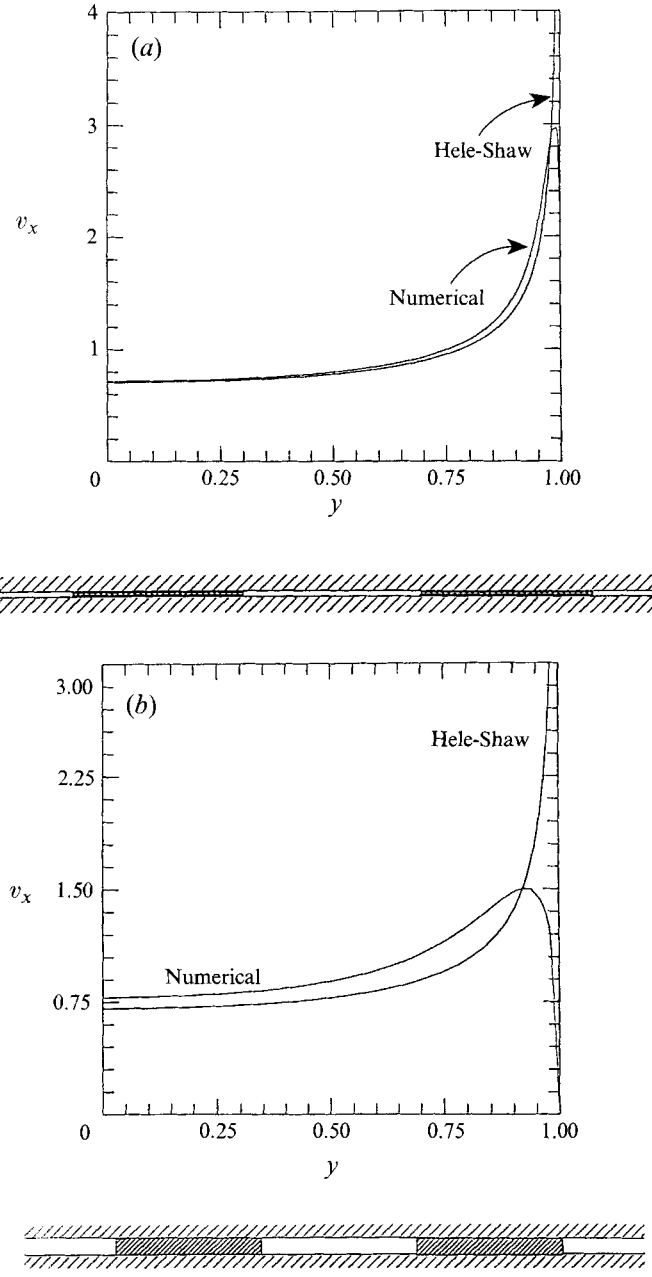

FIGURE 3(*a*,*b*). For caption see facing page.

in v_x is about 10% for $N = 12$ and $M = 50$. In this case, the length of the barrier is much greater than the width of orifice, and there is almost no interaction between orifices. This type of flow could be more conveniently described by a model for the flow past an infinite plate with a single slit between two parallel walls. The present solution provides accurate results for all values of B provided $D < 5$.

Table 2 shows the convergence for the friction factor f_b. Convergence to three significant figures is shown for all three values of B. The convergence of the solution

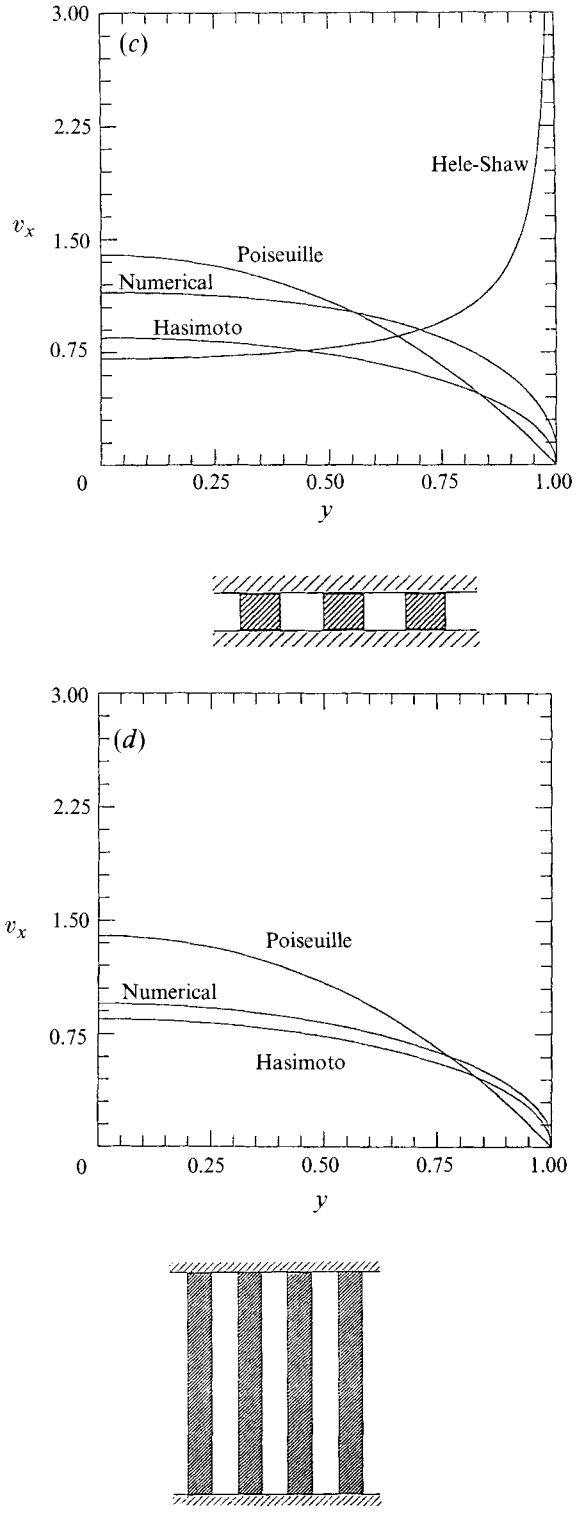

FIGURE 3. Velocity profiles at the orifice opening, $x = 0$, in the midplane, $z = 0$, for $D = 2$: (*a*) $B = 0.02$, (*b*) $B = 0.1$, (*c*) $B = 1$, (*d*) $B = 10$. Sketches of the corresponding cross-section at $x = 0$ with barriers shaded are drawn to scale below the figure for easy visualization.

for global parameters is thus an order of magnitude greater than for the local velocity for the same values of M and N.

4.2. *Velocity field*

Once the unknown coefficients A_{nm} in the general solution (15) are determined, the velocity of the fluid can be evaluated at any spatial point. As noted in the introduction we are particularly interested in investigating the flow characteristics of the orifice entrance profile for the junction strand barriers described in Tsay *et al.* (1989) and Weinbaum *et al.* (1992). In the latter study the entrance profile for the flow past a periodic barrier was assumed to be that of a Poiseuille flow in a $2B' \times 2d'$ rectangular duct. The present results show that for B in the observed physiological range, $0.1 < B < 0.5$, this approximation is poor and will need to be corrected.

The numerical solutions presented herein can be compared with asymptotic solutions for several limiting cases. One limiting case is $B \ll 1$ and $(D-1)/B$ of $O(1)$ or larger. For this case the flow is reasonably approximated by the Hele-Shaw potential flow solution given in §3. A second limiting case, $B \gg 1$, corresponds to Hasimoto's two-dimensional solution (1959) describing the flow through periodic slits in an infinite plane. The third limit, $D-1 \ll 1$, represents obstacles that are widely separated. This solution should be similar to Lee & Fung's (1969) solution for the flow past a single cylindrical post confined in a channel. By comparing our more general solution with these asymptotic solutions at the corresponding limits, the new solution can be verified while at the same time the practical limits of validity for these asymptotic solutions established.

Figures 3(*a*) and 3(*b*) demonstrate the corresponding velocity profiles in the plane of the orifice for Stokes flow and Hele-Shaw flow for $B = 0.02$ and $B = 0.1$ for $D = 2$ in the midplane, $z = 0$. One observes that the velocity profiles for Stokes flow agree closely with the Hele-Shaw profiles, especially for $B = 0.02$, except for a narrow region of $O(B')$ near the edge of the barrier. In this narrow region the Stokes solution reaches a maximum and then decreases rapidly to zero, while the Hele-Shaw solution tends to infinity. These figures reveal that the Hele-Shaw potential flow solution is a reasonable approximation for $B < 0.1$. The maximum in the orifice entrance profile near $y = 1$ disappears entirely at $B \sim 0.5$, result not shown.

Figure 3(*d*) compares the entrance velocity profiles in the orifice plane of the numerical solution, Hasimoto's solution and Poiseuille flow in a rectangular duct for $B = 10$ and $D = 2$ in the midplane, $z = 0$. We can see that the numerical solution closely agrees with Hasimoto's solution at this limiting case as expected, while the Poiseuille solution for $z = 0$ closely approximates a parabola. The difference between the profiles is qualitatively similar to the difference between Sampson's profile for a circular orifice and fully established Poiseuille flow in a circular tube in which the Sampson profile is much blunter. In Dagan, Pfeffer & Weinbaum (1982) it is shown that for a finite-length circular pore whose length is greater than one diameter the entrance profile is closely approximated by the average of the two profiles. This suggests that for a barrier of finite thickness a profile that is the average of Hasimoto's solution and the rectangular pore profile may be a good approximation provided the barrier thickness is greater than d'.

Figure 3(*c*) compares the velocity profiles at the orifice for the numerical solution, the Hele-Shaw solution, Hasimoto's solution and Poiseuille flow in a $2B' \times 2d'$ infinite rectangular tube for the case $B = 1$ and $D = 2$ in the midplane, $z = 0$. We observe that neither Hele-Shaw nor Hasimoto's solutions are satisfactory approximations. The Poiseuille duct flow velocity profile is the best of the three approximate profiles.

Figures 3(*a–d*) reveals the strong dependence of the entrance profile on the aspect ratio B'/d'. For $B'/d' \ll 1$ the velocity has a minimum at the centreline, a maximum near the edge of the barrier and then decreases sharply to satisfy the no-slip boundary condition. The behaviour is analogous to a boundary layer in high-Reynolds-number flow except that here the mechanism is not inertia but a geometrical effect. This behaviour differs from the classical Stokes solutions of Sampson (1891) and Hasimoto (1958) for the flow through zero-thickness orifices of circular or elliptic cross-section or periodic slits in an infinite plane wall where the maximum velocity is at the orifice centre. As the aspect ratio increases, the peak edge velocity decreases and the minimum velocity at the centre of the orifice increases. For B'/d' of $O(1)$ or greater, the maximum velocity occurs at the centreline. For B'/d' of $O(1)$ the profiles are similar to the classical solutions for rectangular duct flow. The new solution clearly shows the transition in behaviour from the Hele-Shaw potential flow limit to Hasimoto's two-dimensional limiting behaviour as B increases from $1 \gg B$ to $B \gg 1$.

Figure 4(*a–d*) illustrates the solutions for $D = 1.1$, barrier width small compared to slit width. In the limit $D \to 1$ this represents the flow past a single barrier. These solutions exhibit the same qualitative behaviour as B increases as the solutions for the flow past a single cylindrical post confined between two plates. The latter profiles are shown in figure 2 of Lee & Fung (1969).

In figures 5(*a*) and 5(*b*), the complete velocity field in the midplane $z = 0$ for two different limiting cases, $B = 0.05$ and $B = 10$, for $D = 2$ are plotted. It is interesting to observe the substantial differences in the flow fields between these two cases, especially near the edge of the barrier, although the barrier geometry is identical in a top-view.

4.3. *The friction coefficient*

In figure 6, the friction coefficient f_b for the Stokes flow and Hele-Shaw potential flow solutions are plotted against the parameter $B/(D-1)$ representing the distance between two plates non-dimensionalized by the barrier width for values of D of 1.01, 1.1, 2, and 5. Also shown is the drag coefficient from Lee & Fung (1969) for the flow past a circular cylindrical post confined between two plates. As expected, the solutions for the Stokes flow (solid lines) asymptotically approach the solutions for Hele-Shaw potential flow (dashed lines) for $B \ll 1$ at different D. Furthermore, figure 6 provides numerical criteria based on the parameters $B/(D-1)$ and D as to when the Hele-Shaw potential flow approximation will be valid. f_b decreases nearly linearly with $B/(D-1)$ for $B/(D-1) \ll 1$ and then asymptotically approaches a constant that depends on D as $B/(D-1)$ increases. As anticipated, the smaller the barrier, the smaller the drag is. When D is very close to 1, and the barrier width is small compared with the width of the opening, one expects the solution to asymptotically approach that past a single obstacle. In this limit one anticipates that the drag should be nearly the same for obstacles of different cross-section but with the same frontal area, as observed, for example, for the flow past a sphere and a disk. This prediction is confirmed by figure 6, which shows the close agreement between the curve at $D = 1.1$ (or $D = 1.01$) and the curve for a single cylinder of radius equal to the half-width of the barrier between the parallel plates given in Lee & Fung (1969).

5. Biological application

The solutions presented in this study have been very useful in formulating a more realistic model for the flow through the junction strand in the intercellular clefts of capillary endothelium. The recent study of the junction strand structure in frog

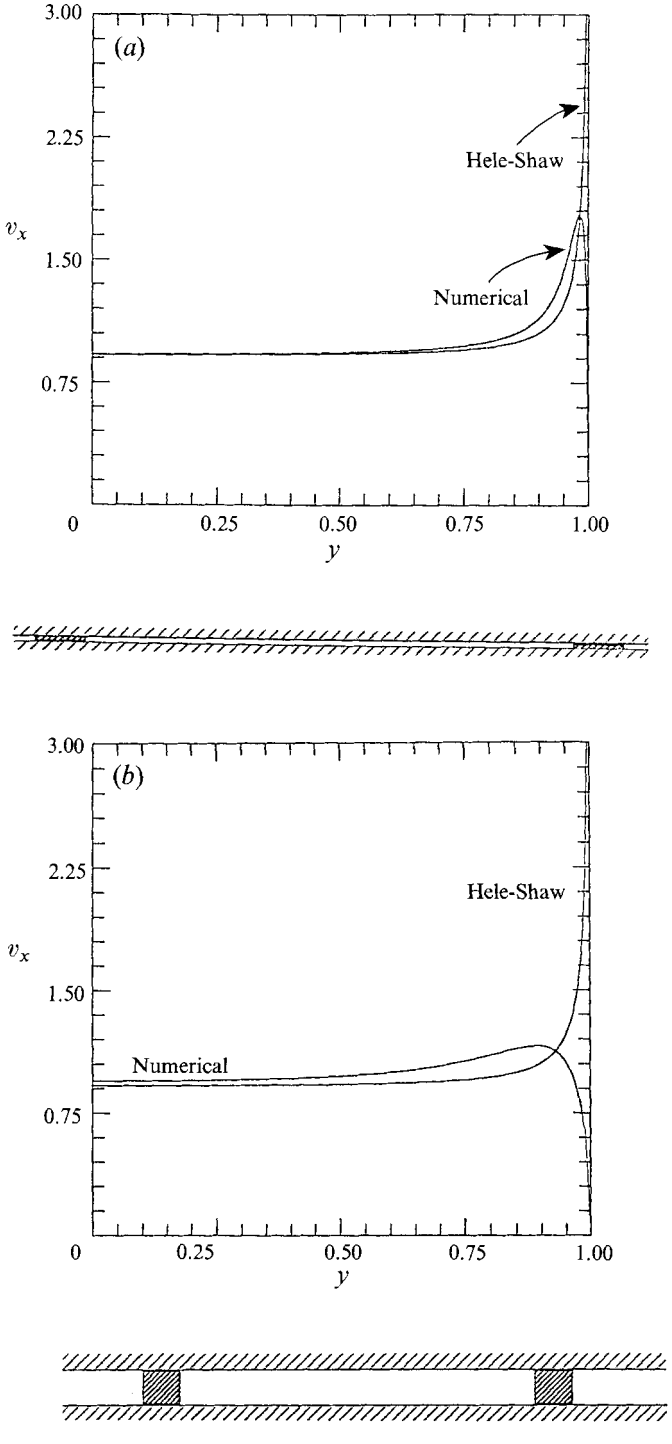

FIGURE 4(*a*,*b*). For caption see facing page.

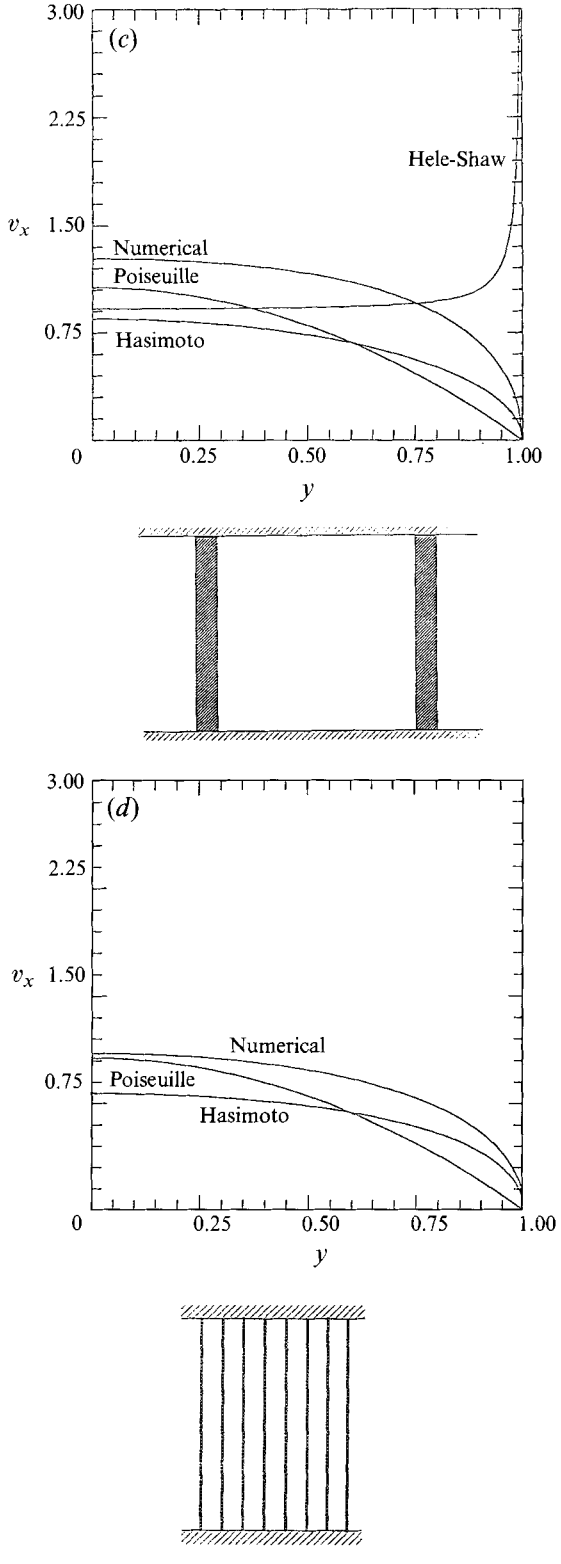

FIGURE 4. Velocity profiles at the orifice opening, $x = 0$, in the midplane, $z = 0$, for $D = 1.1$: (*a*) $B = 0.02$, (*b*) $B = 0.1$, (*c*) $B = 1$, (*d*) $B = 10$. Sketches of the corresponding cross-section at $x = 0$ with barriers shaded are drawn to scale below the figure for easy visualization.

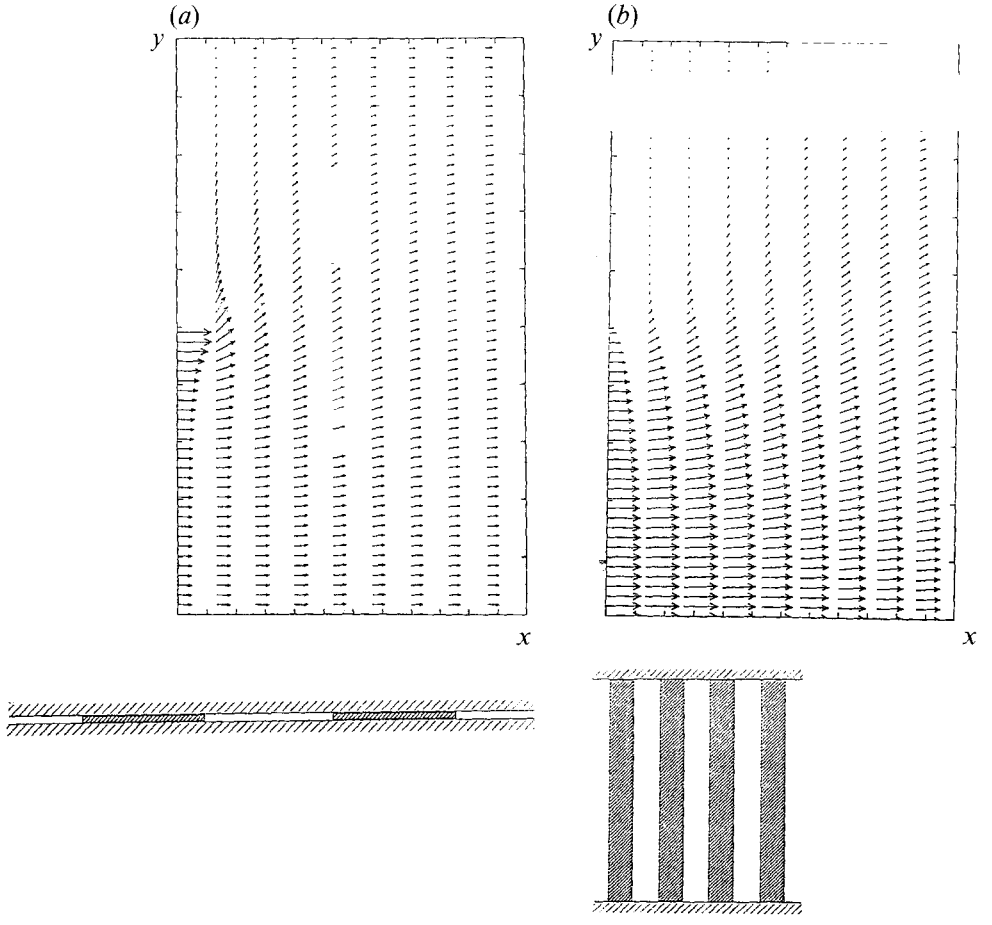

FIGURE 5. Velocity field in the midplane, $z = 0$, with the geometry of the cross-section shown below with barriers shaded for $D = 2$: (*a*) $B = 0.05$, (*b*) $B = 10$.

mesentery, Adamson & Michel (1993), has provided average values for the key geometric parameters in the model. For this tissue $B' = 20$ nm, $d' = 150$ nm and $D' = 2640$ nm. Thus the average aspect of the orifice opening $B = 0.133$ and the dimensionless spacing between orifices $D = 17$. Comparison of the velocity profiles for $B = 0.1$ and $D = 2$ and 5 (latter not shown) reveals that the profiles are insensitive to D for $D > 2$ and thus the solution in figure 3(*b*) is representative of the orifice entrance profile at the junction strand discontinuity for frog mesentery. In an earlier study (Weinbaum *et al.* 1992), a Poiseuille flow solution for flow in a long rectangular duct with the same cross-sectional aspect ratio B was used to estimate the entrance profile fore and aft of the junction strand. It is clear from the profiles in figure 3 that the Hele-Shaw profile is a more suitable representation. Similarly, the results for the drag coefficient in figure 6 reveal that the additional drag due to the junction strand can be well approximated by a simple Hele-Shaw flow since for the above geometric parameters $B/(D-1) = 0.004$. This simplified Hele-Shaw analysis is used in both the Appendix by Parker *et al.* to Adamson & Michel (1993), where a simple model is proposed for the flow through an isolated orifice in a junction strand, and the most recent study by Fu, Tsay & Weinbaum (1994), in which a more complete three-dimensional model for the flow through an intercellular cleft is developed which

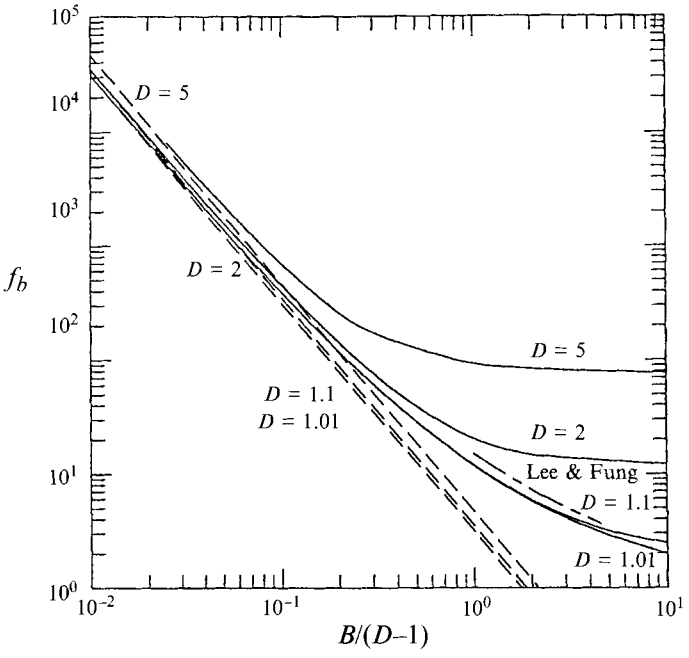

FIGURE 6. The drag coefficient f_b is plotted against $B/(D-1)$ for $D = 1.01$, 1.1, 2, 5. The solid line indicates the numerical solution for Stokes flow, equation (21). The dashed line represents the Hele-Shaw potential flow solution, equation (32). The short-long dashed line corresponds to the solution for flow past a single cylinder confined in a channel, Lee & Fung (1969).

includes a finite region at the entrance to the cleft with cross-bridging fibre matrix components as well as a junction strand with orifice-like breaks. The matrix in the latter model provides the molecular filter and determines the reflection coefficient for different-size solutes.

At present there are no definitive measurements for the geometric parameters in other tissues. It is generally accepted that $2B'$ is approximately 20 nm for capillary clefts in most tissue. However, the measured filtration coefficient for mammalian muscle tissue is typically at least five times lower than frog mensentery. It is not clear whether this reduced filtration coefficient is because the break width $2d'$ is significantly smaller or the spacing between breaks, $2D'$, is much larger than in frog mesentery. The appropriate orifice entrance profile should lie somewhere between the representative results shown in figures 3(*b*) and 3(*c*).

6. Concluding comments

The truncated series solution developed in this paper converges rapidly for all B provided $D < 5$. Solutions for $D > 5$ are probably more efficiently obtained by considering the flow through a single isolated orifice although the shape of the velocity profiles would not differ significantly from those shown in figure 3 for $D = 2$ at the same value of B. Comparison with the Hele-Shaw potential flow solution for the limiting case $B \ll 1$ shows that the latter approximation provides good accuracy for $B < 0.1$. In contrast to the classical orifice solutions of Sampson and Hasimoto, the maximum velocity need not occur on the centreline. There is a transition from the Hele-Shaw potential flow ($B \ll 1$) to the viscous two-dimensional flow ($B \gg 1$)

behaviour as the aspect ratio of the orifice is increased. Numerical results indicate that the resistance coefficient f_b decreases rapidly and then gradually levels off to a constant as the parameter $B/(D-1)$ increases. The transition and value of the constant are a function of D. The solutions for the biological application which motivated this study, the flow through the junction strand barrier in vascular interendothelial clefts, can be reasonably approximated by the Hele-Shaw solution for frog mesentery, but may require the full solution for junction strand breaks in other tissues.

This research was supported by NIH grant NHLBI-HL44485.

REFERENCES

ADAMSON, R. H. & MICHEL, C. C. (with an Appendix by Parker, K. H., Phillips, G. C. & Wang, W.) 1993 *J. Physiol.* **466**, 303.

BUNDGAARD, M. 1984 *J. Ultrastruct. Res.* **88**, 1.

DAGAN, Z., PFEFFER, R. & WEINBAUM, S. 1982 *J. Fluid Mech.* **122**, 273.

FU, B. M., TSAY, R. Y. & WEINBAUM, S. 1994 A junction-orifice-fiber entrance layer model for capillary permeability with application to frog mesentery. *ASME J. Biomech. Engng* (in press).

HASIMOTO, H. 1958 *J. Phys. Soc. Japan* **13**, 633.

HELE-SHAW, H. S. 1898 *Nature* **58**, 34.

LEE, J. S. 1969 *J. Biomech.* **2**, 187.

LEE, J. S. & FUNG, Y. C. 1969 *J. Fluid Mech.* **37**, 657.

SAMPSON, R. A. 1891 *Phil. Trans. R. Soc. Lond.* A **182**, 449.

SANGANI, A. S. & ACRIVOS, A. 1982 *Intl J. Multiphase Flow* **8**, 193.

THOMPSON, B. W. 1968 *J. Fluid Mech.* **31**, 397.

TSAY, R. & WEINBAUM, S. 1991 *J. Fluid Mech.* **226**, 125.

TSAY, R., WEINBAUM, S. & PFEFFER, R. 1989 *Chem. Engng Commun.* **82**, 67.

WEINBAUM, S., TSAY, R. & CURRY, F. E. 1992 *Microvascular Res.* **44**, 85.

ZAUDERER, S. 1989 *Partial Differential Equations of Applied Mathematics*, 2nd edn. Wiley.